

## Fast Accurate State Measurement with Superconducting Qubits

Evan Jeffrey, Daniel Sank, J. Y. Mutus, T. C. White, J. Kelly, R. Barends, Y. Chen, Z. Chen, B. Chiaro, A. Dunsworth, A. Megrant, P. J. J. O'Malley, C. Neill, P. Roushan, A. Vainsencher, J. Wenner, A. N. Cleland, and John M. Martinis\*

*Department of Physics, University of California, Santa Barbara, California 93106-9530, USA*

(Received 19 December 2013; published 15 May 2014)

Faster and more accurate state measurement is required for progress in superconducting qubit experiments with greater numbers of qubits and advanced techniques such as feedback. We have designed a multiplexed measurement system with a bandpass filter that allows fast measurement without increasing environmental damping of the qubits. We use this to demonstrate simultaneous measurement of four qubits on a single superconducting integrated circuit, the fastest of which can be measured to 99.8% accuracy in 140 ns. This accuracy and speed is suitable for advanced multiqubit experiments including surface-code error correction.

DOI: [10.1103/PhysRevLett.112.190504](https://doi.org/10.1103/PhysRevLett.112.190504)

PACS numbers: 03.67.Lx, 85.25.Hv

Maintaining a system's quantum coherence longer than its constituent parts is a major goal of quantum information. Protocols realizing this property, known as fault tolerance, require high fidelity entangling operations (gates) and fast, accurate quantum state measurement. Recent experiments with superconducting qubits have shown gates at the  $\sim 99\%$  fidelity threshold of a fault tolerant protocol known as the surface code [1–6], but the state measurement used in those experiments was not yet accurate or fast enough to be used in the full protocol.

In this Letter, we demonstrate a multiplexed qubit state detector and use it to implement measurement at the surface code threshold. As this state detector is based on the same circuit architecture that has been shown to produce high fidelity gates, it can be readily integrated into future experimental realizations of quantum fault tolerance with the surface code.

Fast and accurate measurement of superconducting qubits is a major challenge because damping introduced by the measurement apparatus creates tension between the measurement speed and the induced qubit energy relaxation time  $T_1$ . In transmon qubits [7] where the qubit state is measured by probing the state dependent frequency shift of an auxiliary linear resonator [8–10], coupling to the environment through the resonator leads to qubit damping via the Purcell effect [11]. The resonator-environment coupling, characterized by a leakage rate  $\kappa_r$ , must be large enough to get photons into and out of the resonators quickly, but weak enough to prevent environmental damping from lowering  $T_1$ . A prior work showed that a notch filter introduced between the resonator and environment suppresses the Purcell effect resulting in higher  $T_1$ , but measurement speed and accuracy were not studied [12]. Subsequent experiments, including those focused on multiqubit gates, have not used filters and have thus remained limited by the Purcell effect, forcing the use of

measurement times too slow for realization of fault tolerant protocols. Other recent experiments demonstrating a variety of novel effects related to state measurement [13–17] have focused on measurement of single bits of classical information, and have worked either with the measurement always on or have had speeds limited by the measurement resonator's transient turn-on time. The cyclic nature of fault tolerant protocols like the surface code requires fast transient response so that the measurement can be switched off during coherent manipulations to avoid continuously collapsing the qubit state. Thus we were motivated to investigate the possibility of fast state measurement in a multiqubit system.

We present here a measurement system based on a single-pole bandpass filter and use it to implement multi-qubit state measurement at high speed. We introduce a design formula based on the  $\kappa_r T_1$  product that characterizes the tension between the transient response rate of the measurement resonator  $\kappa_r$  and the maximum qubit  $T_1$  due to environmental damping. The bandpass filter design increases the  $\kappa_r T_1$  limit to  $\sim 6700$ , with  $\kappa_r = 1/(19 \text{ ns})$  in the fastest of four qubits. Based on these results, we expect that an optimized design could reach  $\kappa_r = 1/(10 \text{ ns})$  while allowing a  $T_1$  above  $100 \mu\text{s}$ . We find that the bandpass filter allows four qubit simultaneous measurement with intrinsic fidelities reaching 99% in less than 200 ns after the start of the measurement pulse.

We achieve this fast measurement by integrating a bandpass filter into a multiplexed resonator system [18]. The device, shown in Fig. 1(a), has four qubit-resonator pairs, designed to test the performance of different compromises between measurement speed and environmentally limited  $T_1$ . Design and fabrication parameters for these qubits are listed in the Supplemental Material [19]. The filter is implemented as a quarter wave ( $\lambda/4$ ) coplanar waveguide resonator embedded directly into the feed line.

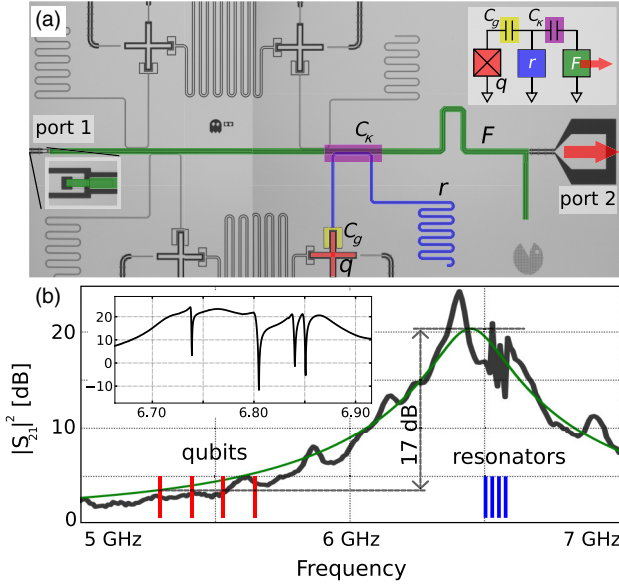


FIG. 1 (color online). Device layout and frequency response. (a) Micrograph of the device with lumped element model (inset). The qubits  $q$  are coupled through a capacitor  $C_g$  to the voltage antinode of the  $\lambda/4$  measurement resonator  $r$ . The resonators are coupled via capacitors  $C_k$  to the filter resonator  $F$ . The red arrow indicates the path by which photons leave the filter through a wire bond (not shown) and enter an amplification chain. (b) Transmission spectrum  $S_{21}$  of the detector. Transmission measured on a test chip is shown by the heavy (black) curve, and a Lorentzian fit is shown by the thin (green) curve. The measurement resonators are in the passband where the transmission is large, whereas the qubits are off resonance and thus protected from the environment. The inset shows a detail of the spectrum from the chip used in this experiment. Each dip in the transmission curve comes from one measurement resonator. Values for  $S_{21}$  are plotted with an arbitrary offset in the vertical scale.

Interruption of the feed line by a capacitor [port 1 in Fig. 1(a)] imposes a voltage antinode, while a ground connection at a distance  $\lambda/4$  imposes a voltage node. The resulting standing wave mode creates a bandpass filter as shown in Fig. 1(b). By placing the measurement resonator frequencies but not the qubit frequencies in the pass band, the measurement resonators are strongly coupled to the environment without damping the qubits. The measurement signal couples out of the filter into the measurement environment through a tap near the voltage node. The energy leakage rate, and thus the quality factor of the filter  $Q_F$ , is set by the fraction of the total voltage at this tap-off point; we designed for  $Q_F = 30$ , which gives enough bandwidth for several measurement resonators while allowing high qubit  $T_1$ .

Each qubit's resonator is connected in parallel to this common filter through a capacitance  $C_k$ , and each qubit is connected to its resonator by a capacitance  $C_g$  to give a qubit-resonator coupling strength  $g/2\pi$  between 50 and 150 MHz.

The design was based on an analytic theory of the  $\kappa_r T_1$  product, which characterizes the limit on the measurement rate  $\kappa_r$  for a given environmentally limited qubit lifetime  $T_1$  (see the Supplemental Material [19]). For the unfiltered case the product is constrained by  $\kappa_r T_1 \leq (\Delta/g)^2$ , where  $\Delta \equiv \omega_q - \omega_r$  is the qubit-resonator detuning. The product cannot be effectively increased by raising  $\Delta$  because this requires a corresponding increase in  $g$  to maintain a measurable dispersive phase shift [7,10]. Introducing a bandpass filter increases the  $\kappa_r T_1$  product to (see the Supplemental Material [19])

$$\kappa_r T_1 \leq \left(\frac{\Delta}{g}\right)^2 \left(\frac{\omega_r}{\omega_q}\right) \left(\frac{2\Delta}{\omega_r/Q_F}\right)^2. \quad (1)$$

The final factor in Eq. (1) allows faster measurement without lowering  $T_1$ ; for fixed  $\kappa_r$ ,  $\Delta$ , and  $g$  the new limit exceeds the unfiltered one by a factor of  $4Q_F^2 \Delta^2 / \omega_q^2 \approx 100$ . This factor nearly matches the observed difference in system power transmission  $|S_{21}|^2$  between the qubit and resonator frequencies, as shown by the vertical arrow in Fig. 1(b). Device parameters are given in the Supplemental Material [19]. With target parameters  $\omega_r/2\pi = 6.765$  GHz,  $\omega_q/2\pi = 5.5$  GHz,  $g/2\pi = 86$  MHz, and  $\kappa_r^{-1} = 37$  ns, we compute an expected 1.2 ms, which greatly exceeds the  $T_1$  limit imposed by other decay channels in the experiment. While this prevents explicit observation of the Purcell limit in this experiment, it is more relevant to future experiments in which the measurement system should not limit qubit coherence.

We use a multitone signal, generated with a custom microwave frequency arbitrary waveform generator, to simultaneously probe each of the measurement resonators [18]. Each qubit imparts a state dependent phase shift to one frequency component of the measurement pulse. The phase shifted signal is amplified by a Josephson parametric amplifier (paramp) with 600 MHz of near quantum limited bandwidth and a 1 dB compression point of  $-107$  dBm [23]. The large bandwidth and saturation power of the amplifier was critical in our ability to simultaneously measure all four qubits. The signal is filtered by a 250 MHz Gaussian filter before it is digitized, and the amplitudes and phases for each frequency component are extracted. For each frequency this yields a point in the quadrature (IQ) plane that depends on the state dependent phase shift imparted by the qubit.

Each measurement pulse consists of a short (25–50 ns) high-power transient to quickly ring up the resonator, followed by a sustain pulse (150 ns), as shown in Fig. 2(a). The resonator rings down freely, with a decay rate  $\kappa_r = \omega_r/Q_r$ , which is the slowest part of the sequence as shown in Fig. 2(b). The qubit can be coherently manipulated again after several resonator decay time constants. The pulse time of 150 ns plus 7 times  $\kappa_r$  yields a total cycle time of 410 ns. This is 2 orders of magnitude

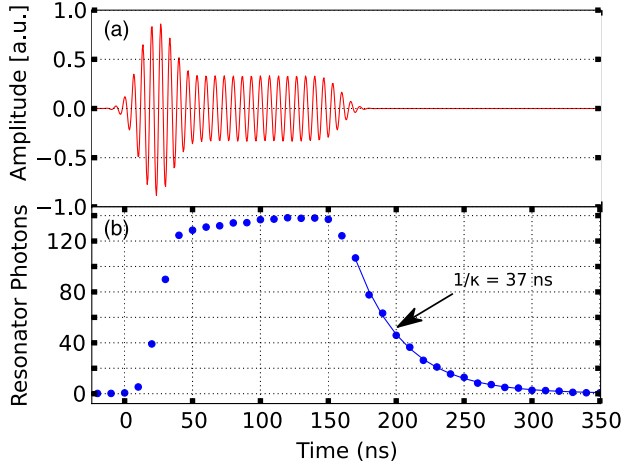


FIG. 2 (color online). Measurement pulse shape and resonator photon occupation. (a) Measurement pulse produced by the arbitrary waveform generator for a single qubit (real quadrature). (b) Time dependent population of the measurement resonator as measured by the ac Stark shift. This shows the initial 25 ns strong drive, which quickly rings up the resonator, the sustain pulse, and the free ringdown with time constant  $1/\kappa_r = 37$  ns. This corresponds to a resonator  $Q_r$  of 1561.

below typical qubit lifetimes (20–40  $\mu$ s), making the measurement viable in a surface code system.

In Fig. 3 we show the IQ points for many single-shot measurement events in which the qubit was prepared in the  $|0\rangle$  and  $|1\rangle$  states. Each point is generated by integrating from the beginning of the demodulated measurement signal (time = 0 in Fig. 2). Shots are recorded as  $|0\rangle$  or  $|1\rangle$

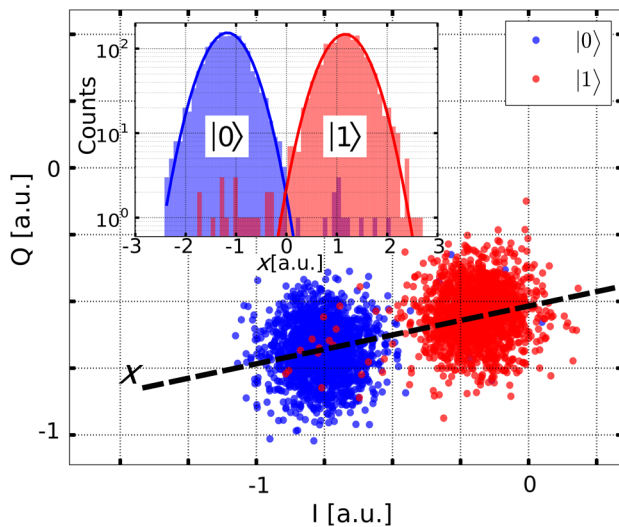


FIG. 3 (color online). Single shot measurement events for one qubit after 140 ns pulse integration. Points in the wrong cluster are due to unwanted qubit transitions. The inset shows histograms of the IQ points projected onto line connecting the  $|0\rangle$  and  $|1\rangle$  clouds. Heavy lines are Gaussian fits to the histograms and are used for computing the separation fidelity.

according to which cloud’s centroid is nearest to the resulting IQ value.

At equilibrium, our qubits have a 5%–10% probability to be in the excited state. To separate this effect from other sources of error, we use heralding [14]; we begin each sequence with an initial measurement and discard trials where the qubit does not start in the ground state.

Focusing on a single qubit-resonator pair  $Q_2$ , we measure the qubit and resonator frequencies spectroscopically, and then find the probe frequency for which the two IQ clouds corresponding to the qubit ground and excited states are maximally separated. All subsequent measurement pulses on this qubit use this frequency. The photon number occupation in the resonator was calibrated by measuring the ac Stark shift of the qubit [8]. We then varied the photon number to find the largest signal to noise ratio possible without introducing unwanted qubit state transitions. We found that the qubit state was preserved to within 1% as long as the photon number was kept less than approximately 4 times larger than the “critical photon number” defined as  $n_c = (\Delta/g)^2/4$  [10]. At photon numbers above  $4n_c$  we observed a sharp onset of unwanted qubit state transitions.

Measuring the qubits’  $T_1$  versus frequency, we find that in all four designs there was no observable suppression of  $T_1$  at the smallest  $\Delta/2\pi$  achievable (approximately 800 MHz), indicating that the filter successfully isolated the qubits from the environment. All four qubits were operated with  $T_1$  values between 10 and 12  $\mu$ s.

In Fig. 3 we show results for a single qubit at a single integration time. For each point we prepare either  $|0\rangle$  or  $|1\rangle$  with the absence or presence of a  $\pi$  pulse, and then turn on the measurement. We integrate the measurement signal for 140 ns beginning at the start of the pulse when there are zero photons in the resonator. We characterize the measurement in two ways. First, we consider the “separation fidelity”  $F_s$ , which characterizes the distinguishability of the Gaussian fits to the IQ clouds of the two qubit states. Because of the finite separation and widths of the clouds, a point drawn from the IQ distribution for either state may be erroneously identified as the other state. We define  $F_s$  as the probability that a point drawn from the fitted distribution for either state is correctly identified. Here we find  $F_s = 99.8\%$ . Second, we define the total measurement fidelities  $\{F_{|x\rangle}\}$  as the probability that a qubit prepared as  $|x\rangle$  is correctly identified. This includes unwanted qubit state transitions during the measurement. While these errors arise fundamentally from the qubit, we regard them as measurement errors here because they can be reduced with faster measurement. We find  $F_{|0\rangle} = 99.3\%$  and  $F_{|1\rangle} = 98.7\%$ , just at the surface code threshold of  $\sim 99\%$  [5,6].

While separation fidelity is improved by collecting more scattered photons, this requires longer measurement and thus incurs more qubit errors. To fully characterize this time dependence we measured the separation and total fidelities as functions of integration time, as shown in Fig. 4. We use

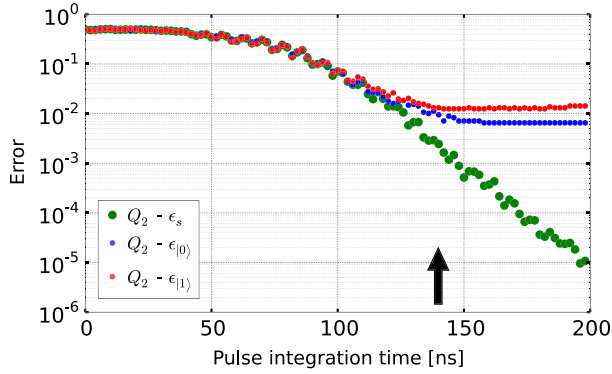


FIG. 4 (color online). Measurement errors versus pulse integration time for one qubit. Large (green) circles show the separation errors  $\epsilon_s = 1 - F_s(t)$  while the dark (blue) and light (red) small circles show  $\epsilon_{|0\rangle}(t)$  and  $\epsilon_{|1\rangle}(t)$ , respectively. The vertical arrow indicates the time slice at 140 ns represented in Fig. 3.

the same procedure as in Fig. 3 but vary the upper limit in the time integration to generate a time series of IQ clouds from which we extract  $F_s(t)$ ,  $F_{|0\rangle}(t)$ , and  $F_{|1\rangle}(t)$ . We used  $F_s(t)$  as an empirical optimal window and reintegrate the data weighted by this window. For clarity we plot the errors, defined as  $\epsilon \equiv 1 - F$ , instead of the fidelities. The separation fidelity reaches 99% at 124 ns after the pulse start, and improves exponentially with increasing integration time.

The data with near constant slope show that, after the initial transient of the measurement pulse,  $\epsilon_s(t)$  decreases at a rate of approximately one decade per 25 ns. This rate depends on the ratio between the detected photon flux and the system noise (SNR). Loss of any scattered photons before they are detected lowers the SNR. As each scattered photon carries partial information on the qubit state it also causes qubit dephasing. This provides a way to measure the fraction of lost photons: we compare the experimental SNR to the dephasing induced by the measurement (see the Supplemental Material [19] and Ref. [24]). In this way we find a quantum efficiency of  $-9$  dB, of which  $-3$  dB can be attributed to using a phase insensitive amplifier (see the Supplemental Material [19] and Ref. [22]). We note that, as it would improve only the steady state SNR but not the transient response, increasing the quantum efficiency would improve the measurement performance only slightly.

The state errors decrease along with the separation error for the first 100 ns before they begin to saturate. This saturation can be explained by considering two deleterious qubit state transition processes. We have measured that in equilibrium our qubits experience upward  $|0\rangle \rightarrow |1\rangle$  transitions with a rate of  $\Gamma_{\uparrow} \approx 1/100 \mu\text{s}$ , which result in excited state populations of 5% to 10%. These transitions lead to state preparation errors; with 500 ns between the heralding and final measurements, we expect 0.5% repopulation of the excited state before the start of the final measurement. This nearly explains the saturation of  $F_{|0\rangle}$  at 99.3%. The

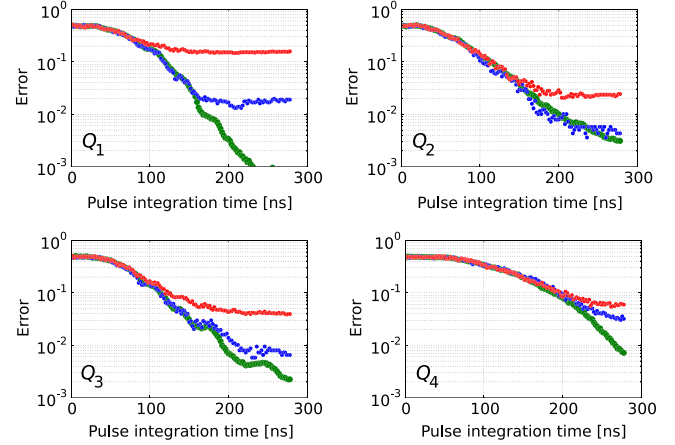


FIG. 5 (color online). Simultaneous measurement of four qubits. Separation and actual state fidelities are shown as in Fig. 4. All four qubits exhibit fast measurement, with three of them reaching 99% fidelity in 200 ns. Small ripples on qubits  $Q_1$  and  $Q_3$  were caused by spectral leakage.

second error process is the usual qubit energy relaxation; a qubit transition before the halfway point of the measurement leads to an error. With a measurement time of 140 ns and  $T_1 = 10 \mu\text{s}$  we expect an extra 0.7% loss in excited state population yielding an expected limit of 98.8%. This agrees well with the measured  $F_{|1\rangle}$  saturation at 98.7%.

We also measured all four qubits simultaneously, as shown in Fig. 5. Three of the four qubits reached 99% separation fidelity within 200 ns. The fourth device, which had the most conservative  $\kappa_r T_1$  product, reached 99% separation fidelity at 266 ns. In order to prevent saturation of the paramp with four simultaneous measurement tones, we reduced the drive power relative to the single qubit measurement. This required an increase in the measurement time, which led to slightly lower fidelity than was achieved with a single qubit.

For qubits  $Q_2$  and  $Q_4$  the performance is nearly as good as for the single qubit case. The small degradation of performance comes from increased qubit transitions during the longer measurement time. Qubits  $Q_1$  and  $Q_3$  show lower  $F_{|1\rangle}$ . As shown in the inset of Fig. 1 the measurement resonators for qubits  $Q_1$  and  $Q_3$  are closely spaced in frequency (13 MHz). This close spacing adversely affects the frequency discrimination step of the measurement via spectral leakage, leading to increased measurement error. In addition the measurement photons induce large qubit frequency shifts (200–300 MHz) via the ac Stark effect. This causes the qubits to cross through resonance with material defects and lose  $|1\rangle$  population. We were able to work around this problem with careful choice of operating frequency in qubits  $Q_2$ ,  $Q_3$ , and  $Q_4$ , but limited total available frequency space led to degraded performance in  $Q_1$ . This problem would be substantially mitigated in devices constructed with epitaxial Al films grown on plasma cleaned substrates [25] as this was shown to

produce qubit frequency spectra with a significant reduction in defects [26].

In conclusion, we have demonstrated fast and accurate multiqubit state measurement in superconducting qubits. Amplifier saturation power is a key metric for system performance, and further improvements in amplifiers would allow the bandpass filter design to scale to even higher numbers of qubits. Other improvements could be made by considering the effect of optimized demodulation windows [27]. This system is suitable for more complex experiments with larger numbers of qubits, and meets the threshold requirements for measurement in the surface code. A full demonstration of fault tolerance will require combining this work with high fidelity gates [1] and scaling to even larger numbers of qubits.

This work was supported by the Office of the Director of National Intelligence (ODNI), Intelligence Advanced Research Projects Activity (IARPA), through Army Research Office Grants No. W911NF-09-1-0375 and No. W911NF-10-1-0334. All statements of fact, opinion, or conclusions contained herein are those of the authors and should not be construed as representing the official views or policies of IARPA, the ODNI, or the U.S. Government. E. J. and D. S. contributed equally to this work.

---

\*martinis@physics.ucsb.edu

- [1] R. Barends, J. Kelly, A. Megrant, A. Veitia, D. Sank, E. Jeffrey, Y. Chen, B. Chiaro, J. Mutus, C. Neill *et al.*, *Nature (London)* **508**, 500 (2014).
- [2] J. M. Chow, J. M. Gambetta, E. Magesan, S. J. Srinivasan, A. W. Cross, D. W. Abraham, N. A. Masluk, B. R. Johnson, C. A. Ryan, and M. Steffen, [arXiv:1311.6330](https://arxiv.org/abs/1311.6330).
- [3] O.-P. Saira, J. Groen, J. Cramer, M. Meretska, G. de Lange, and L. DiCarlo, *Phys. Rev. Lett.* **112**, 070502 (2014).
- [4] S. Gustavsson, O. Zwiier, J. Bylander, F. Yan, F. Yoshihara, Y. Nakamura, T. P. Orlando, and W. D. Oliver, *Phys. Rev. Lett.* **110**, 040502 (2013).
- [5] A. G. Fowler, M. Mariantoni, J. M. Martinis, and A. N. Cleland, *Phys. Rev. A* **86**, 032324 (2012).
- [6] R. Raussendorf and J. Harrington, *Phys. Rev. Lett.* **98**, 190504 (2007).
- [7] J. Koch, T. M. Yu, J. Gambetta, A. A. Houck, D. I. Schuster, J. Majer, A. Blais, M. H. Devoret, S. M. Girvin, and R. J. Schoelkopf, *Phys. Rev. A* **76**, 042319 (2007).
- [8] D. I. Schuster, A. Wallraff, A. Blais, L. Frunzio, R.-S. Huang, J. Majer, S. M. Girvin, and R. J. Schoelkopf, *Phys. Rev. Lett.* **94**, 123602 (2005).
- [9] A. Wallraff, D. I. Schuster, A. Blais, L. Frunzio, J. Majer, M. H. Devoret, S. M. Girvin, and R. J. Schoelkopf, *Phys. Rev. Lett.* **95**, 060501 (2005).
- [10] A. Blais, R.-S. Huang, A. Wallraff, S. M. Girvin, and R. J. Schoelkopf, *Phys. Rev. A* **69**, 062320 (2004).
- [11] E. Purcell, *Phys. Rev.* **69**, 674 (1946).
- [12] M. Reed, B. Johnson, A. Houck, L. DiCarlo, J. Chow, D. Schuster, L. Frunzio, and R. Schoelkopf, *Appl. Phys. Lett.* **96**, 203110 (2010).
- [13] R. Vijay, D. H. Slichter, and I. Siddiqi, *Phys. Rev. Lett.* **106**, 110502 (2011).
- [14] J. E. Johnson, C. Macklin, D. H. Slichter, R. Vijay, E. B. Weingarten, J. Clarke, and I. Siddiqi, *Phys. Rev. Lett.* **109**, 050506 (2012).
- [15] D. H. Slichter, R. Vijay, S. J. Weber, S. Boutin, M. Boissonneault, J. M. Gambetta, A. Blais, and I. Siddiqi, *Phys. Rev. Lett.* **109**, 153601 (2012).
- [16] K. Murch, S. Weber, C. Macklin, and I. Siddiqi, *Nature (London)* **502**, 211 (2013).
- [17] J. M. Chow, L. DiCarlo, J. M. Gambetta, A. Nunnenkamp, L. S. Bishop, L. Frunzio, M. H. Devoret, S. M. Girvin, and R. J. Schoelkopf, *Phys. Rev. A* **81**, 062325 (2010).
- [18] Y. Chen, D. Sank, P. O'Malley, T. White, R. Barends, B. Chiaro, J. Kelly, E. Lucero, M. Mariantoni, A. Megrant *et al.*, *Appl. Phys. Lett.* **101**, 182601 (2012).
- [19] See Supplemental Material at <http://link.aps.org/supplemental/10.1103/PhysRevLett.112.190504> for derivation of Eq. (1) with comparison to numerics, device parameters, discussion of the photon collection efficiency, and a detailed diagram of the experimental setup, which includes Refs. [20–22].
- [20] D. Esteve, M. H. Devoret, and J. M. Martinis, *Phys. Rev. B* **34**, 158 (1986).
- [21] Z. Chen, A. Megrant, J. Kelly, R. Barends, J. Bochmann, Y. Chen, B. Chiaro, A. Dunsworth, E. Jeffrey, J. Y. Mutus *et al.*, *Appl. Phys. Lett.* **104**, 052602 (2014).
- [22] C. M. Caves, *Phys. Rev. D* **26**, 1817 (1982).
- [23] T. C. White, J. Mutus, R. Barends, J. Kelly, A. Megrant, D. Sank, E. Jeffrey, Y. Chen, B. Chiaro, C. Neill *et al.*, [arXiv:1401.3799](https://arxiv.org/abs/1401.3799).
- [24] Y. Makhlin, G. Schön, and A. Shnirman, *Rev. Mod. Phys.* **73**, 357 (2001).
- [25] A. Megrant, C. Neill, R. Barends, B. Chiaro, Y. Chen, L. Feigl, J. Kelly, E. Lucero, M. Mariantoni, P. O'Malley *et al.*, *Appl. Phys. Lett.* **100**, 113510 (2012).
- [26] R. Barends, J. Kelly, A. Megrant, D. Sank, E. Jeffrey, Y. Chen, Y. Yin, B. Chiaro, J. Mutus, C. Neill *et al.*, *Phys. Rev. Lett.* **111**, 080502 (2013).
- [27] J. Gambetta, W. A. Braff, A. Wallraff, S. M. Girvin, and R. J. Schoelkopf, *Phys. Rev. A* **76**, 012325 (2007).